Technical University of Denmark

DTU

Visualization of and Software for Omnibus Test Based Change Detected in a Time Series of Polarimetric SAR Data

Nielsen, Allan Aasbjerg; Conradsen, Knut; Skriver, Henning; Canty, Morton J.

Link back to DTU Orbit

DTU Library
Technical Information Center of Denmark

Visualization of and Software for Omnibus Test Based Change Detected in a Time Series of Polarimetric SAR Data

Allan A. Nielsen, Knut Conradsen, Henning Skriver & Morton J. Canty

Visualization of and software for omnibus test based change detected in a time series of polarimetric SAR data

Allan A. Nielsen, Knut Conradsen, Henning Skriver, and Morton J. Canty[*]

October 25, 2017

Abstract

Based on an omnibus likelihood ratio test statistic for the equality of several variance-covariance matrices following the complex Wishart distribution and a factorization of this test statistic with associated p-values, change analysis in a time series of multilook polarimetric SAR data in the covariance matrix representation is carried out. The omnibus test statistic and its factorization detect if and when change occurs. Using airborne EMISAR and spaceborne RADARSAT-2 data this paper focuses on change detection based on the p-values, on visualization of change at pixel as well as segment level, and on computer software.
http://www.imm.dtu.dk/pubdb/p.php?6914.

Cette étude effectue une analyse sur le changement d'une série temporelle de données multivisées et polarimétriques de radar à synthèse d'ouverture (RSO) représentée sous forme de matrice de covariance. Cette analyse est basée sur 1) un rapport de vraisemblance omnibus pour l'égalité de plusieurs matrices de variance-covariance suivant la distribution de Wishart complexe et 2) une factorisation de celle-ci avec les valeurs-p associées. La statistique de test omnibus et la factorisation correspondante signalent l'occurrence d'un changement. Par moyen de EMISAR aéroportée et RADARSAT-2, cette étude se porte sur la détection de changement en s'appuyant sur les valeurs-p, la visualisation de changement au niveau des pixels et des segments, et des logiciels informatiques.

Introduction

In the analysis of remote sensing data, a very important aspect is the analysis of spatio-temporal dynamcis including change detection over time. There is an interesting literature on change detection in polarimetric SAR imagery, see for example Dierking, & Skriver (2002); Qong (2004); Moser, Serpico, & Vernazza (2007); Moser, & Serpico (2009); Formont, Pascal, Vasile, Ovarlez, & Ferro-Famil (2011); Erten, Reigber, & Ferro-Famil (2012); Marino, Cloude, & Sanchez-Lopez (2013); Liu, Zhang, Wang, & Wu (2014); Carotenuto, Maio, Clemente, & Soraghan (2015); Deledalle, Denis, Tupin, Reigber, & Jäger (2015); Carotenuto, Maio, Clemente, Soraghan, & Alfano (2016); Akbari et al. (2016); Yang, Yang, Yan, Song, & Xia (2016).

In Conradsen, Nielsen, Schou, & Skriver (2003) we described a likelihood ratio test statistic for equality of two variance-covariance matrices following the complex Wishart distribution and its application to change detection between two time points, see also Canty (2014). We also used this test statistic for edge detection, see Schou, Skriver, Nielsen, & Conradsen (2003). Special aspects (for example multi-frequency analysis) with computer code were dealt with in Nielsen, Conradsen, & Skriver (2015).

In Conradsen, Nielsen, & Skriver (2016) we described a likelihood ratio test statistic Q for equality of a series of variance-covariance matrices following the complex Wishart distribution. We also described a factorization of $Q = \prod_{j=2}^{k} R_j$ where the test statistics Q and R_j determine if and when a difference occurs. This we used for pixel-wise change detection in a series of multilook polarimetric synthetic aperture radar (SAR) image data in the covariance matrix representation, see van Zyl, & Ulaby (1990). Additionally, based on approximate distributions of the test statistics we gave p-values for Q and R_j to determine significance levels for change/no-change.

---

[*]A. A. Nielsen and K. Conradsen, DTU Compute, Department of Applied Mathematics and Computer Science, Technical University of Denmark, DK-2800 Kgs. Lyngby, Denmark. H. Skriver, DTU Space, National Space Institute, Technical University of Denmark, DK-2800 Kgs. Lyngby, Denmark. M. J. Canty is an emeritus from the Jülich Research Center, D-52428 Jülich, Germany. Corresponding author: Allan A. Nielsen, e-mail alan@dtu.dk, internet http://people.compute.dtu.dk/alan, phone +45 4525 3425, fax +45 4588 1397.

Generally, one could say that whether you want to characterize a small difference in pixel values as a change event or a random fluctuation, is a philosophical question, it is your choice. In statistically based analysis this choice translates into a choice of significance level.

Because Q tests for equality in all matrices simultaneously, it is termed an omnibus test statistic. Testing all matrices simultaneously makes Q able to detect more subtle, slowly developing changes than the more often used pairwise test statistics.

In this paper we further analyze the change patterns as found by the methods described in Conradsen et al. (2016). Specifically, we give an update scheme to handle the situation where you have analyzed a sequence of images up to time point $j - 1$ already and you get new data from time point j, we mention/describe Matlab and Python software to perform the analysis, and we give visualization examples of the change detected. This is done in the form of change at field or segment level, and per pixel occurrence of the first and last change as well as the number of changes. Also an RGB representation of per pixel change is given.

Here the methods are demonstrated by means of airborne EMISAR, see Madsen, Christensen, Skou, & Dall (1991); Christensen et al. (1998) (L-band) data and spaceborne RADARSAT-2[1] (C-band) data. The methods are well suited for analysis of spaceborne ALOS, COSMO-SkyMed, Sentinel-1, TerraSAR-X, and Yaogan data also.

The following sections very briefly sketch the main results from Conradsen et al. (2016), briefly describe the results output from the analysis, give per pixel and per field change visualization examples, and sketch Matlab and Python code.

Test Statistics and Their Distributions

This section very briefly recapitulates the main results from Conradsen et al. (2016) on change detection in a series of covariance matrix representation multilook SAR data, see van Zyl, & Ulaby (1990).

Test for equality of several complex covariance matrices

For the logarithm of the likelihood ratio test statistic Q for testing whether a series of $k \geq 2$ complex variance-covariance matrices $\boldsymbol{\Sigma}_i$ are equal, i.e., $\boldsymbol{\Sigma}_1 = \boldsymbol{\Sigma}_2 = \cdots = \boldsymbol{\Sigma}_k$ we get (for the real case see Anderson (2003); for the case with two complex matrices see Conradsen et al. (2003); Schou et al. (2003))

$$\ln Q = n\{pk \ln k + \sum_{i=1}^{k} \ln |\boldsymbol{X}_i| - k \ln |\sum_{i=1}^{k} \boldsymbol{X}_i|\}. \tag{1}$$

Here $|\cdot|$ denotes the determinant, n is the equivalent number of looks, the $\boldsymbol{X}_i$ (and the $\boldsymbol{\Sigma}_i$) are p by p ($p = 3$ for full pol data, $p = 2$ for dual pol data, and $p = 1$ for single channel power data), and the $\boldsymbol{X}_i = n\hat{\boldsymbol{\Sigma}}_i = n\langle \boldsymbol{C} \rangle_i$ follow the complex Wishart distribution, i.e., $\boldsymbol{X}_i \sim W_C(p, n, \boldsymbol{\Sigma}_i)$.

Because Q tests for equality in all matrices simultaneously, it is termed an omnibus test statistic.

In Conradsen et al. (2016) we give p-values $1 - P\{-2\rho \ln Q \leq z\}$ for Q to determine significance levels for no-change (where ρ is an auxiliary variable and $z = -2\rho \ln q_{\text{obs}}$ where q_{obs} is the observed value of Q).

Test for equality of first $j \leq k$ matrices

If the above $\ln Q$ test statistic shows that we cannot reject the hypothesis $\boldsymbol{\Sigma}_1 = \boldsymbol{\Sigma}_2 = \cdots = \boldsymbol{\Sigma}_k$, there is no change over the time span covered by the data. If we can reject the hypothesis, there is change at some time point. To find that time point, we test whether the first j ($1 < j \leq k$) complex variance-covariance matrices $\boldsymbol{\Sigma}_i$ are equal, i.e., given that $\boldsymbol{\Sigma}_1 = \boldsymbol{\Sigma}_2 = \cdots = \boldsymbol{\Sigma}_{j-1}$, then the logarithm of the likelihood ratio test statistic R_j for testing $\boldsymbol{\Sigma}_j = \boldsymbol{\Sigma}_1$ is

$$\ln R_j = n\{p(j \ln j - (j-1) \ln(j-1)) \\ + (j-1) \ln |\sum_{i=1}^{j-1} \boldsymbol{X}_i| + \ln |\boldsymbol{X}_j| - j \ln |\sum_{i=1}^{j} \boldsymbol{X}_i|\}. \tag{2}$$

---

[1]The official RADARSAT-2 web site is http://www.asc-csa.gc.ca/eng/satellites/radarsat2/.

Table 1: Part of the structure `wc` as output from code `wcRjl` for an example with data from six time points.

	$t_1 = \cdots = t_6$	$t_2 = \cdots = t_6$	$t_3 = \cdots = t_6$	$t_4 = \cdots = t_6$	$t_5 = t_6$
Omnibus	$Q^{(1)}$: `wc(1).P(1)`	$Q^{(2)}$: `wc(2).P(1)`	$Q^{(3)}$: `wc(3).P(1)`	$Q^{(4)}$: `wc(4).P(1)`	$Q^{(5)}$: `wc(5).P(1)`
$t_1 = t_2$	$R_2^{(1)}$: `wc(1).P(2)`				
$t_2 = t_3$	$R_3^{(1)}$: `wc(1).P(3)`	$R_2^{(2)}$: `wc(2).P(2)`			
$t_3 = t_4$	$R_4^{(1)}$: `wc(1).P(4)`	$R_3^{(2)}$: `wc(2).P(3)`	$R_2^{(3)}$: `wc(3).P(2)`		
$t_4 = t_5$	$R_5^{(1)}$: `wc(1).P(5)`	$R_4^{(2)}$: `wc(2).P(4)`	$R_3^{(3)}$: `wc(3).P(3)`	$R_2^{(4)}$: `wc(4).P(2)`	
$t_5 = t_6$	$R_6^{(1)}$: `wc(1).P(6)`	$R_5^{(2)}$: `wc(2).P(5)`	$R_4^{(3)}$: `wc(3).P(4)`	$R_3^{(4)}$: `wc(4).P(3)`	$R_2^{(5)}$: `wc(5).P(2)`

Furthermore, the R_j constitute a factorization $Q = \prod_{j=2}^{k} R_j$ or

$$\ln Q \;=\; \sum_{j=2}^{k} \ln R_j. \tag{3}$$

In Conradsen et al. (2016) we also gave p-values $1 - P\{-2\rho_j \ln R_j \leq z_j\}$ for R_j to determine significance levels for no-change (where ρ_j are auxiliary variables and $z_j = -2\rho_j \ln r_{j,\text{obs}}$ where $r_{j,\text{obs}}$ are the observed values of R_j).

Update of change detected from time $j-1$ to time j

Equation (2) shows that we can calculate $\ln R_j$ based on $\boldsymbol{X}_j$ and either all previous data $\boldsymbol{X}_i$, $i = 1, \ldots, j-1$ or the sum of all previous data $\sum_{i=1}^{j-1} \boldsymbol{X}_i$. To do the former we need to store all previous data, to do the latter we need to store their sum and, since we need the logarithm of the determinant of the sum, preferably also this log-determinant.

Q and R_j Based Change Analysis

This analysis builds a structure of change for each pixel: first we analyze for change over all time points, then for change over all time points omitting the first time point, then for change over all time points omitting the first two time points, etc. The change structure is illustrated in Table 1 for an example with data from six time points. If change is detected comparing for example t_2 and t_3 in the "$t_1 = \cdots = t_6$" column, the remaining tests in that column are invalid and we continue in the column starting with detection of change from t_3. This will leave the "$t_2 = \cdots = t_6$" column irrelevant. Continuing like this we can build up the change pattern for all pixels over all time points, see also Conradsen et al. (2016).

Matlab code `wcRjl` (briefly described in the section on software outputs the structure `wc` a part of which is shown in Table 1. The first column indicates which tests are performed for the row in question. The second column shows $P\{-2\rho \ln Q^{(1)} \leq z\}$ ("Omnibus" row) or $P\{-2\rho_j \ln R_j^{(1)} \leq z_j\}$, $j = 2, \ldots, 6$ for all time points t_1 through t_6. The third column shows $P\{-2\rho \ln Q^{(2)} \leq z\}$ ("Omnibus" row) or $P\{-2\rho_j \ln R_j^{(2)} \leq z_j\}$, $j = 2, \ldots, 5$ for time points t_2 through t_6. The fourth column shows $P\{-2\rho \ln Q^{(3)} \leq z\}$ ("Omnibus" row) or $P\{-2\rho_j \ln R_j^{(3)} \leq z_j\}$, $j = 2, \ldots, 4$ for time points t_3 through t_6, etc. For a test for $R_j^{(\ell)}$ to be valid, all previous tests for $R_i^{(\ell)}$, $i = 2, \ldots, j-1$ must show equality.

$R_2^{(\ell)}$, $\ell = 1, \ldots, k-1$ is the pairwise (or marginal or "non-omnibus") test statistics for equality between consecutive time points t_ℓ and $t_{\ell+1}$ (as described in Conradsen et al. (2003)). Note, that for the last column $Q = R_2$.

$P\{-2\rho \ln Q^{(\ell)} \leq z\}$ is stored in `wc(\ell).P(1)`, and $P\{-2\rho_j \ln R_j^{(\ell)} \leq z_j\}$ is stored in `wc(\ell).P(j)`.

Change Visualization Examples

To illustrate results from analyses by means of the Matlab code mentioned in the sction on software we use full polarimetry EMISAR L-band data acquired in 1998 over a Danish agricultural test site on $t_1 = 21$ March (dataset

3

ACCEPTED MANUSCRIPT

L62), $t_2 = 17$ April (dataset L63), $t_3 = 20$ May (dataset L64), $t_4 = 16$ June (dataset L65), $t_5 = 15$ July (dataset L68), and $t_6 = 16$ August (dataset L74). The 13-look images are 1024 rows by 1024 columns 5 m pixels, see Conradsen et al. (2016) for more details.

To generate the desired change structure call

```
wc = wcRjl(cat(4,L62,L63,L64,L65,L68,...
    L74),13,'full',false);
```

for a structure without storing the pixelwise sum of all data and the logarithm of the determinant of the sum (`false` in the call). Alternatively, to store these quantities call either (you need not specify the polarization)

```
wc = wcRjl(cat(4,L62,L63,L64,L65,L68,...
    L74),13,'full');
```

or for example (again the pol specification is not needed)

```
wc = wcRjl(cat(4,L62,L63),13,'full');
wc = wcRjl_updt(wc,L64,13,'full');
wc = wcRjl_updt(wc,L65,13,'full');
wc = wcRjl_updt(wc,L68,13,'full');
wc = wcRjl_updt(wc,L74,13,'full');
```

Per pixel change visualization

Given the structure `wc` as output from `wcRjl` or `wcRjl_updt` (we need `wc.P` only) and a threshold for the change probability, the Matlab function `wcWhen` finds when change(s) occurred on a pixel basis. Following the call

```
[c,nsets] = wcWhen(wc,0.9999);
```

this code finds when the first change occurred at a change probability significance level of 99.99% (corresponding to a no-change probability significance level of 0.01%)

```
[maxch,changeFirst] = max(c,[],3);
changeFirst(maxch==0) = 0;
```

For the six L-band EMISAR data sets also analyzed in Conradsen et al. (2016) this code

```
figure, imshow(changeFirst,[]), axis off
h = colorbar('southoutside');
set(h,'XTick',0:(nsets-1))
colormap jet0
```

generates Figure 1 which shows the time point at which the first detected change took place for full polarization data (change probability significance level is 99.99%). "jet0" is Matlab's "jet" colormap with the first entry set to black. Since we expect to analyze also very long time series for which a continuous colour scale is to be preferred, we choose to use that colour scale here also with six time points only.

This code finds when the last/most recent change occurred at a change probability significance level of 99.99% (corresponding to a no-change probability significance level of 0.01%) and generates Figure 2

```
[maxch,changeLast] = ...
    max(c(:,:,(nsets-1):-1:1),[],3);
changeLast = nsets - changeLast;
changeLast(maxch==0) = 0;
figure, imshow(changeLast,[]), axis off
h = colorbar('southoutside');
set(h,'XTick',0:(nsets-1))
colormap jet0
```

This code finds the number of changes/change frequency and generates Figure 3

4

Table 2: Average no-change probabilities for a grass field.

	$t_1 = \cdots = t_6$	$t_2 = \cdots = t_6$	$t_3 = \cdots = t_6$	$t_4 = \cdots = t_6$	$t_5 = t_6$
Omnibus	0.0000	0.0000	0.0000	0.0000	0.0000
$t_1 = t_2$	0.2808				
$t_2 = t_3$	0.0112	0.0638			
$t_3 = t_4$	0.0056	0.0319	0.1244		
$t_4 = t_5$	0.1094	0.2386	0.3879	0.4311	
$t_5 = t_6$	0.0000	0.0000	0.0000	0.0000	0.0000

```
sumc = sum(c,3);
figure, imshow(sumc,[]), axis off
h = colorbar('southoutside');
set(h,'XTick',0:(nsets-1))
colormap jet0
```

As a further example of per pixel change visualization of the same data, this generates Figure 4

```
figure, imshow(single(c(:,:,[1 3 5])))
axis off
```

which shows changes from t_1 to t_2 (in the beginning of the time series) as red, from t_3 to t_4 (in the middle of the time series) as green, and from t_5 to t_6 (in the end of the time series) as blue. This (of course) means that for example yellow areas have changed during time intervals $t_1 - t_2$ and $t_3 - t_4$, white areas have changed during time intervals $t_1 - t_2$, $t_3 - t_4$, and $t_5 - t_6$. Black areas have not changed.

Finally, for illustration the Python scripts were used to perform change analysis of a series of 12 quad polarimetric RADARSAT-2 images acquired near the city of Bonn, Germany between May, 2009 and October, 2010. Figure 7 shows a 400×400-pixel spatial subset of the first image in the series. The dark feature near the center is a flooded sand quarry. The corresponding change frequency map is shown in Figure 8, where there is seen to be a "hot spot" in the sand quarry caused by the continual movement of two dredging arms.

Per field change visualization

Table 2 shows the average no-change probabilities for a field (the field chosen is the grass field also analyzed in Conradsen et al. (2016); it is chosen because the omnibus test statistic detects change not detected by the pairwise test statistics). Figure 5 shows the same probabilities as graphs, one line per column in Table 2. The omnibus test based no-change probabilities shown along with the pairwise no-change probabilities in the bottom plot in Figure 6 are highlighted in yellow. These numbers show that at a 5% significance level the pairwise tests show no change over the time span March to July. Contrary to this the omnibus tests show change between April and May (and also between July and August). If we apply a 1% significance level change is detected between May and June, and between July and August.

As an example of visualization of per field change detection Figure 6 shows mean values in the grass field of the backscatter coefficients and the span (first plot), the determinant of the covariance matrix multiplied by the equivalent number of looks (second plot), the magnitude of the correlation between HH and VV (third plot), and the phase difference between HH and VV for all six acquisitions (fourth plot). The last plot shows the average pairwise and omnibus based no-change probabilities (at a 5% level).

The parameters in Figure 6 can be interpreted in terms of the scattering mechanisms for the grass vegetation. In March and April, the low HV backscatter, the larger VV than HH backscatter, the relatively high correlation coefficient, and some phase difference between HH and VV indicate that the scattering is dominated by surface scattering and some double bounce scattering from the not so dense vegetation. In May, June and July, the higher HV backscatter, the same HH and VV backscatter, the lower correlation coefficient, and a phase difference close to zero indicate volume scattering from the dense vegetation. In August, where the grass has been cut, the parameters

indicate surface scattering, i.e., low HV backscatter, larger VV than HH backscatter, correlation coefficient close to one, and phase difference close to zero. This interpretation matches clearly with the three no-change segments at the 5 % significance level indicated above: 1) March and April, 2) May, June and July, and 3) August.

We expect that plots like these will be even more useful for interpreting change in longer time series where possible periodical, step and impulse changes will be conspicuous.

Finally, we show an example of visualization of per field change detection for the RADARSAT example. Figure 9 shows the sample and theoretical distributions of $-2\rho \ln Q$ and $-2\rho_j \ln R_j$ for a no-change wooded region. Judged visually these compare satisfactorily.

The visualization examples shown in this subsection are field or patch based. However the actual change detection is pixel based. The change detection itself could be patch based also. Following some segmentation of the imagery, after adjustment for the number of looks which will depend on the segment size, the change detection method sketched above could be applied to the segments. This is not pursued further here.

For no-change examples, see the wooded areas in the pixelswise visualizations (most of the black areas in Figures 1, 2, 3, 4, and 8).

Software

Both Matlab and Python code to carry out the analyses described are available.

Matlab Code

Several Matlab functions are available on Allan Nielsen's homepage[2]

- `freadenvisar`,
- `rho_hhvv`,
- `wishart_det`,
- `wishart_change_Q`,
- `wishart_change_Rj`,
- `wcRjl`,
- `wishart_change_Rj_updt`,
- `wcRjl_updt`,
- `wcWhen`,
- `wcPtable`,
- `wclnRtable`.

`freadenvisar` reads covariance matrix polarimetric SAR data (with an ENVI-like header file) from disk and stores them in the order needed for the change detection programs. You may need to change the file names in the code. Also some files are written in row major order and some in column major order, so there may be an issue with transposing the images read.

`rho_hhvv` calculates the complex correlation between HH and VV polarizations (including the phase difference) for full polarimetry, azimuthal symmetry, and dual polarimetry with HH and VV.

`wishart_det` calculates determinants of complex variance-covariance matrices and flags singularity for full polarimetry (including azimuthal symmetry and diagonal only), and dual polarimetry (including diagonal only).

`wishart_change_Q` calculates $\ln Q$ and the p-value to test for equality of $k \geq 2$ covariance matrices in the full and dual polarimetry cases and of single band power data (any polarization). `wishart_change_Q` calculates $\ln Q$ as in (1).

`wishart_change_Rj` calculates $\ln Q$, $\ln R_j$ and the associated p-values to test for equality of covariance matrices in full and dual polarimetry data as well as in single band power data, $k \geq 2$. `wishart_change_Rj` calculates $\ln Q$ as

---

[2]http://people.compute.dtu.dk/alan/ under Software

in (3). This code also exists in a version which reads, processes and writes data from/to disk line-by-line making it useful for large datasets that do not fit into computer memory.

wcRjl is a wrapper which calls `wishart_change_Rj` several times, first with data from all time points (which generates output for the second column of Table 1), then with data from all time points omitting the first, (which generates output for the third column of Table 1), then with data from all time points omitting the two first (which generates output for the fourth column of Table 1), etc. The output is a structure `wc` which contains

- `wc(ℓ).lnR` ($\ln Q$ and $\ln R_j$; $\ln Q$ is stored in `lnR(:,:,1)`, $\ln R_2$ in `lnR(:,:,2)`, etc.),

- `wc(ℓ).f` (f),

- `wc(ℓ).rho` (ρ and ρ_j),

- `wc(ℓ).omega2` (ω_2 and ω_{2j}), and

- `wc(ℓ).P` (p-values, stored in the same fashion as $\ln Q$ and $\ln R_j$).

For $\ell = 1$ all time points are considered, for $\ell = 2$ all time points omitting the first are considered, for $\ell = 3$ all time points omitting the two first are considered, etc. The structure may optionally contain

- `wc(ℓ).sumMat` (the sum $\sum_{i=1}^{j} \boldsymbol{X}_i$) and

- `wc(ℓ).logDet` (the logarithm of the determinant of this sum mentioned in the section on updating of change).

For large data sets the structure `wc` takes up a lot of computer memory. You may want to output `wc.P` only. Also you may want to store this in four as opposed to eight byte precision.

`wishart_change_Rj_updt`: given data from k time points `wishart_change_Rj_updt` based on new data in $\boldsymbol{X}_{k+1}$, calculates $\ln R_{k+1}$, p-values and auxiliary variables (f etc.) for full and dual polarimetry data as well as for single band power data.

`wcRjl_updt` like wcRjl is a wrapper. `wcRjl_updt` calls `wishart_change_Rj_updt` several times, first with either data from all time points or the sum of data from all time points (which updates output for the second column of Table 1 with an extra row followed by an update of $\ln Q$ based on Equation (3)), then with either data from all time points or the sum of data from all time points, omitting the first, (which updates output for the third column of Table 1 with an extra row followed by an update of $\ln Q$ based on Equation (3)), then with either data from all time points or the sum of data from all time points, omitting the two first (which updates output for the fourth column of Table 1 with an extra row followed by an update of $\ln Q$ based on Equation (3)), etc. A version called `wcRjl_data_updt` that handles the situation with no storage of the sum $\sum_{i=1}^{j} \boldsymbol{X}_i$ (and the logarithm of the determinant of this sum) mentioned in the section on updating is also available.

`wcWhen` examines the change probabilities (P) in the structure `wc` output by `wcRjl` and outputs all occurrences of change (given a change probability significance level).

`wcPtable` calculates the no-change probabilities $(1 − P)$ from the structure `wc` output by `wcRjl` for a region of interest (ROI) and outputs a table such as Table 1 (or Table 2). It also plots histograms for the no-change probabilities in the ROI. These histograms are flat for a ROI with no change (the distribution of $1 − P$ is uniform). You may input a ROI image or a colour image on which to draw a ROI polygon.

`wclnRtable` calculates $−2\rho \ln Q$ and $−2\rho_j \ln R_j$ from the structure `wc` output by `wcRjl` for a region of interest (ROI) and outputs a table such as Table 1. It also plots sample histograms and theoretical distributions for the these quantities in the ROI. Figure 9 shows that judged visually these two match satisfactorily for a no-change region.

Python Code

Python scripts for (Q and) R_j based change detection are available at Docker Hub[3]. The software package, a so-called *Docker image*, can be pulled and run as a *Docker container* from any host computer which has the *Docker Engine* installed, freely available for Linux, Windows and Mac OS[4]. In addition to a complete Linux environment and all necessary Python prerequisites and scripts for polarimetric SAR change detection, the Docker container encapsulates Python code for speckle filtering and for multivariate estimation of the equivalent number of looks (ENL) of an image in polarimetric matrix format Anfinsen, Doulgeris, & Eltoft (2009). The container also includes the command line interface of the ASF MapReady software for terrain correction and geocoding of SAR images[5]. The user interacts

---

[3]https://hub.docker.com/u/mort/
[4]https://docs.docker.com/
[5]https://www.asf.alaska.edu/data-tools/mapready/

with the software in his or her browser in an IPython notebook served from within the Docker container. Parallel computation on multi-core processors is possible if the user enables the corresponding number of IPython engines. The change detection script is `sar_seq.py`. This script accepts as input a comma-separated list of filenames for the multi-temporal polarimetric image sequence. If required, the images are co-registered to the first image in the sequence and clipped to the same spatial dimensions. Then the per-pixel R_j values for the entire sequence are pre-calculated and their p-values are stored in a memory-mapped array on disk. Both of these steps are run in parallel on IPython engines if available, otherwise they are performed sequentially. Finally the p-value array is scanned at the desired significance level, and four byte arrays having the spatial dimensions of the images are updated recursively in order to generate geo-referenced change maps. These are:

- c_map: the interval in which the most recent significant change occurred (single-band),

- s_map: the interval in which the first significant change occurred (single-band),

- f_map: the frequency of significant changes (single-band), and

- b_map: the interval in which each significant change occurred $((k-1)$-band).

A typical output log is shown below for a sequence of 12 RADARSAT-2 quad polarimetric images. The calculation was performed on an Intel quad core 1.7 GHz processor with four IPython engines enabled.

```
***** Multitemporal PolSAR Change Detection *****
***** Radarsat2 quad or dualpol imagery *********
***** Pre-processed with MapReady ***************
*************************************************
number of images     12
ENL                  12
spatial subset       [300,150,1000,1000]
significance level   0.0001
==========================
Spatial/spectral subsetting
==========================
Fri May 27 17:57:23 2016
Input /home/imagery/...polSAR.tif
elapsed time: 0.855578184128

attempting parallel execution of co-registration ...
available engines [0, 1, 2, 3]
elapsed time for co-registration: 96.2256379128
=============================================
    Multi-temporal SAR Change Detection
=============================================
Fri May 27 17:59:00 2016
First (reference) filename:  ...polSAR_sub.tif
number of images: 12
equivalent number of looks: 12.000000
significance level: 0.00010000
pre-calculating Rj and p-values ...
attempting parallel calculation ...
available engines [0, 1, 2, 3]
ell =  1 2 3 4 5 6 7 8 9 10 11
elapsed time for p-value calculation: 99.2794229984
most recent change map written to: ...sarseq_cmap.tif
frequency map written to: ...sarseq_fmap.tif
bitemporal map image written to: ...sarseq_bmap.tif
first change map written to: ...sarseq_smap.tif
total elapsed time: 200.15645504
```

The complete source code for the Docker image is available on GitHub[6] under the MIT license. Also a tutorial notebook in HTML format can be found on Github[7].

Conclusions

Based on the omnibus test statistic and its factorization for change detection in truly multitemporal, multilook, polarimetric SAR data described in Conradsen et al. (2016), we briefly describe software to perform the analysis, we give per pixel change visualization examples, specifically the time point of the first change, the time point of the last/most recent change, the number of changes/change frequency, and we give an example of an RGB representation of change in the beginning, the middle and the end of the time series analyzed. Also, a per field visualization example which is meant to assist an analyst in determining the type of change is given.

Here, for the grass field selected the pairwise tests showed change at a 5% level between July and August only, whereas the omnibus tests showed change between April and May as well as between July and August. If we choose a 1% level, the change detected between April and May is replaced by change between May and June.

Also an example on omnibus change detection based on a series of quad polarization RADARSAT-2 images is shown. This example shows a "hot spot" in a sand quarry caused by the continual movement of two dredging arms. It also gives an example on the theoretical and sample distributions of the test statistics in a (wooded) no-change region. The two compare satisfactorily.

The accompanying software is expected to be useful to both researchers and practioners working on time series of polarimetric SAR data.

References

Akbari, V., Anfinsen, S. N., Doulgeris, A. P., Eltoft, T., Moser, G., & Serpico, S. B. (2016, Jul.). Polarimetric SAR change detection with the complex Hotelling-Lawley trace statistic. *IEEE Transactions on Geoscience and Remote Sensing*, *54*(7), 3953–3966.

Anderson, T. W. (2003). *An introduction to multivariate statistical analysis* (Third ed.). John Wiley, New York.

Anfinsen, S. N., Doulgeris, A. P., & Eltoft, T. (2009, Nov.). Estimation of the equivalent number of looks in polarimetric synthetic aperture radar imagery. *IEEE Transactions on Geoscience and Remote Sensing*, *47*(11), 3795–3809.

Canty, M. J. (2014). *Image analysis, classification and change detection in remote sensing: With algorithms for ENVI/IDL and Python* (Third ed.). Taylor & Francis, CRC Press.

Carotenuto, V., Maio, A. D., Clemente, C., & Soraghan, J. J. (2015, Jun.). Invariant rules for multipolarization sar change detection. *IEEE Transactions on Geoscience and Remote Sensing*, *53*(6), 3294–3311.

Carotenuto, V., Maio, A. D., Clemente, C., Soraghan, J. J., & Alfano, G. (2016, Jan.). Forcing scale invariance in multipolarization sar change detection. *IEEE Transactions on Geoscience and Remote Sensing*, *54*(1), 36–50.

Christensen, E. L., Skou, N., Dall, J., Woelders, K., Jørgensen, J. H., Granholm, J., & Madsen, S. N. (1998). EMISAR: An absolutely calibrated polarimetric L- and C-band SAR. *IEEE Transactions on Geoscience and Remote Sensing*, *36*, 1852–1865.

Conradsen, K., Nielsen, A. A., Schou, J., & Skriver, H. (2003, Jan.). A test statistic in the complex Wishart distribution and its application to change detection in polarimetric SAR data. *IEEE Transactions on Geoscience and Remote Sensing*, *41*(1), 4–19. Retrieved from http://ieeexplore.ieee.org/Xplore/ RecentIssue.jsp?Punumber=36 (http://www.imm.dtu.dk/pubdb/p.php?1219)

Conradsen, K., Nielsen, A. A., & Skriver, H. (2016, May). Determining the points of change in time series of polarimetric SAR data. *IEEE Transactions on Geoscience and Remote Sensing*, *54*(5), 3007–3024. (http://www.imm.dtu.dk/pubdb/p.php?6825)

Deledalle, C. A., Denis, L., Tupin, F., Reigber, A., & Jäger, M. (2015). NL-SAR: A unified nonlocal framework for resolution-preserving (Pol)(In) SAR denoising. *IEEE Transactions on Geoscience and Remote Sensing*, *53*(4), 2021–2038.

Dierking, W., & Skriver, H. (2002, Mar.). Change detection for thematic mapping by means of airborne multitemporal polarimetric SAR imagery. *IEEE Transactions on Geoscience and Remote Sensing*, *40*(3), 618–636.

---

[6]http://mortcanty.github.io/SARDocker/
[7]http://mortcanty.github.io/src/tutorialsar.html

Erten, E., Reigber, A., & Ferro-Famil, L. (2012, Dec.). A new coherent similarity measure for temporal multichannel scene characterization. *IEEE Transactions on Geoscience and Remote Sensing*, *52*(12), 2839–2851.

Formont, P., Pascal, F., Vasile, G., Ovarlez, J. P., & Ferro-Famil, L. (2011, Jun.). Statistical classification for heterogeneous polarimetric SAR images. *IEEE Journal of Selected Topics in Signal Processing*, *5*(3), 567–576.

Liu, M., Zhang, H., Wang, C., & Wu, F. (2014, Jul.). Change detection of multilook polarimetric SAR images using heterogeneous clutter models. *IEEE Transactions on Geoscience and Remote Sensing*, *50*(7), 7483–7494.

Madsen, S. N., Christensen, E. L., Skou, N., & Dall, J. (1991). The Danish SAR system: Design and initial tests. *IEEE Transactions on Geoscience and Remote Sensing*, *29*, 417–426.

Marino, A., Cloude, S., & Sanchez-Lopez, J. (2013, May). A new polarimetric change detector in radar imagery. *IEEE Transactions on Geoscience and Remote Sensing*, *51*(5), 2986–3000.

Moser, G., & Serpico, S. B. (2009, Jul.). Unsupervised change detection from multichannel SAR data by Markovian data fusion. *IEEE Transactions on Geoscience and Remote Sensing*, *47*(7), 2114–2128.

Moser, G., Serpico, S. B., & Vernazza, G. (2007, Apr.). Unsupervised change detection from multichannel SAR images. *IEEE Geoscience and Remote Sensing Letters*, *4*(2), 278–282.

Nielsen, A. A., Conradsen, K., & Skriver, H. (2015, Aug.). Change detection in full and dual polarization, single- and multi-frequency SAR data. *IEEE Journal of Selected Topics in Applied Earth Observations and Remote Sensing*, *8*(8), 4041–4048. (http://www.imm.dtu.dk/pubdb/p.php?6827)

Qong, M. (2004, Oct.). Polarization state conformation and its application to change detection in polarimetric SAR data. *IEEE Geoscience and Remote Sensing Letters*, *1*(4), 304–307.

Schou, J., Skriver, H., Nielsen, A. A., & Conradsen, K. (2003, Jan.). CFAR edge detector for polarimetric SAR images. *IEEE Transactions on Geoscience and Remote Sensing*, *41*(1), 20–32. `http://ieeexplore.ieee.org` (http://www.imm.dtu.dk/pubdb/p.php?1224)

van Zyl, J. J., & Ulaby, F. T. (1990). Scattering matrix representation for simple targets. In F. T. Ulaby & C. Elachi (Eds.), *Radar polarimetry for geoscience applications*. Artech, Norwood, MA.

Yang, W., Yang, X., Yan, T., Song, H., & Xia, G.-S. (2016). Region-based change detection for polarimetric SAR images using Wishart mixture models. *IEEE Transactions on Geoscience and Remote Sensing*, *54*(11), 6746–6756. (https://doi.org/10.1109/TGRS.2016.2590145)
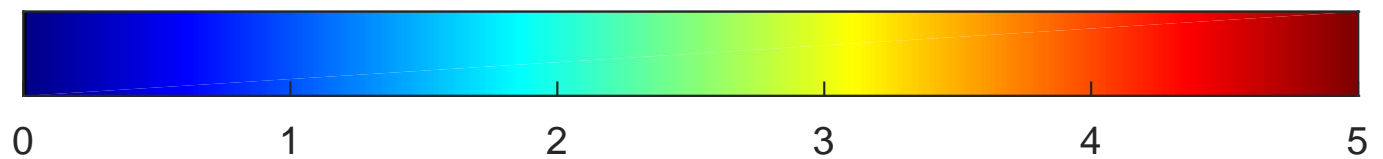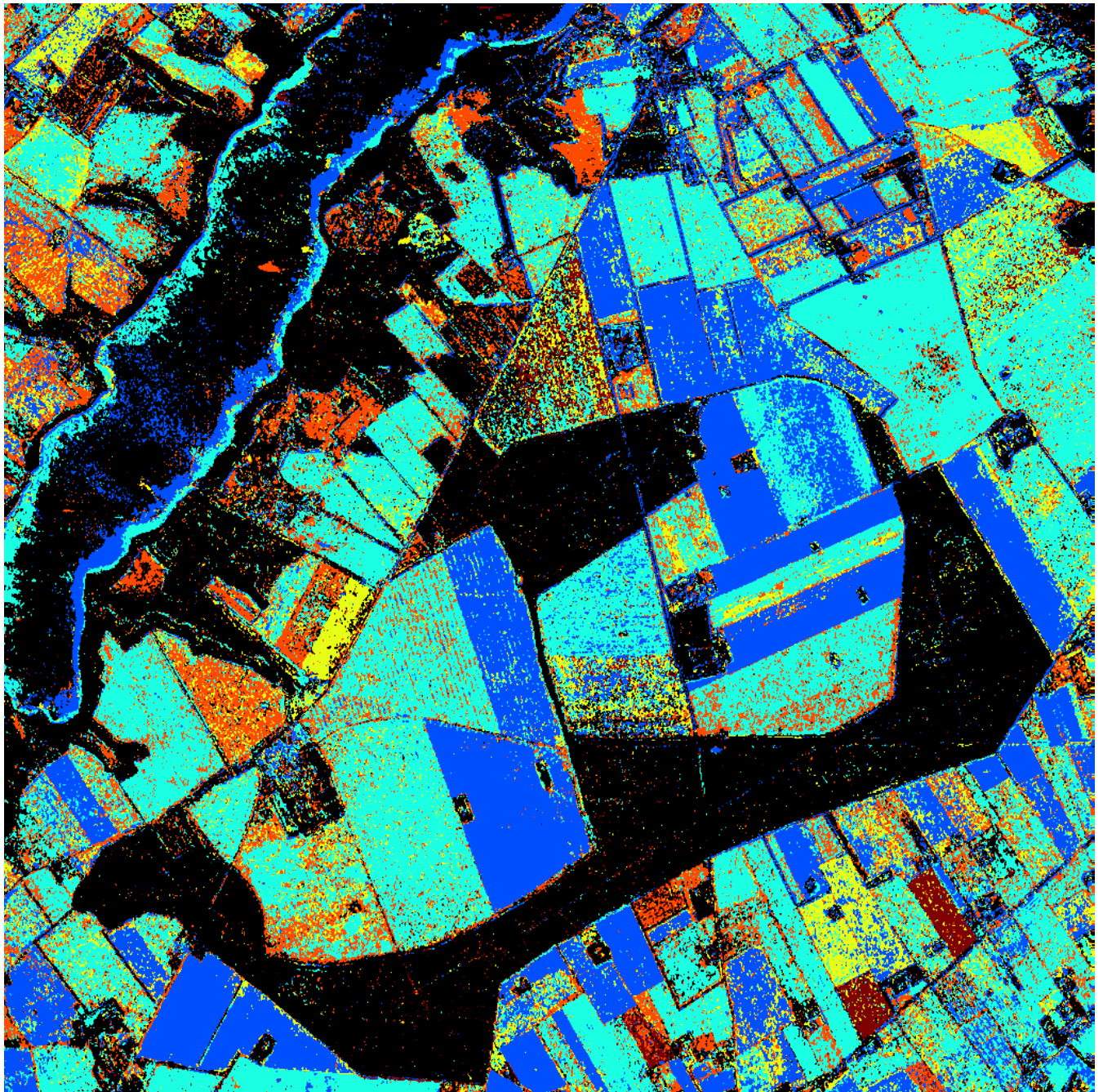
Figure 1: Shows when the first detected change occurred, zero (black) means no change over the time span, one means first change occurred between t_1 and t_2, etc. No change occurred in wooded regions and most of the lake to the north-west. Change probability significance level (for full polarization data) is 99.99%.
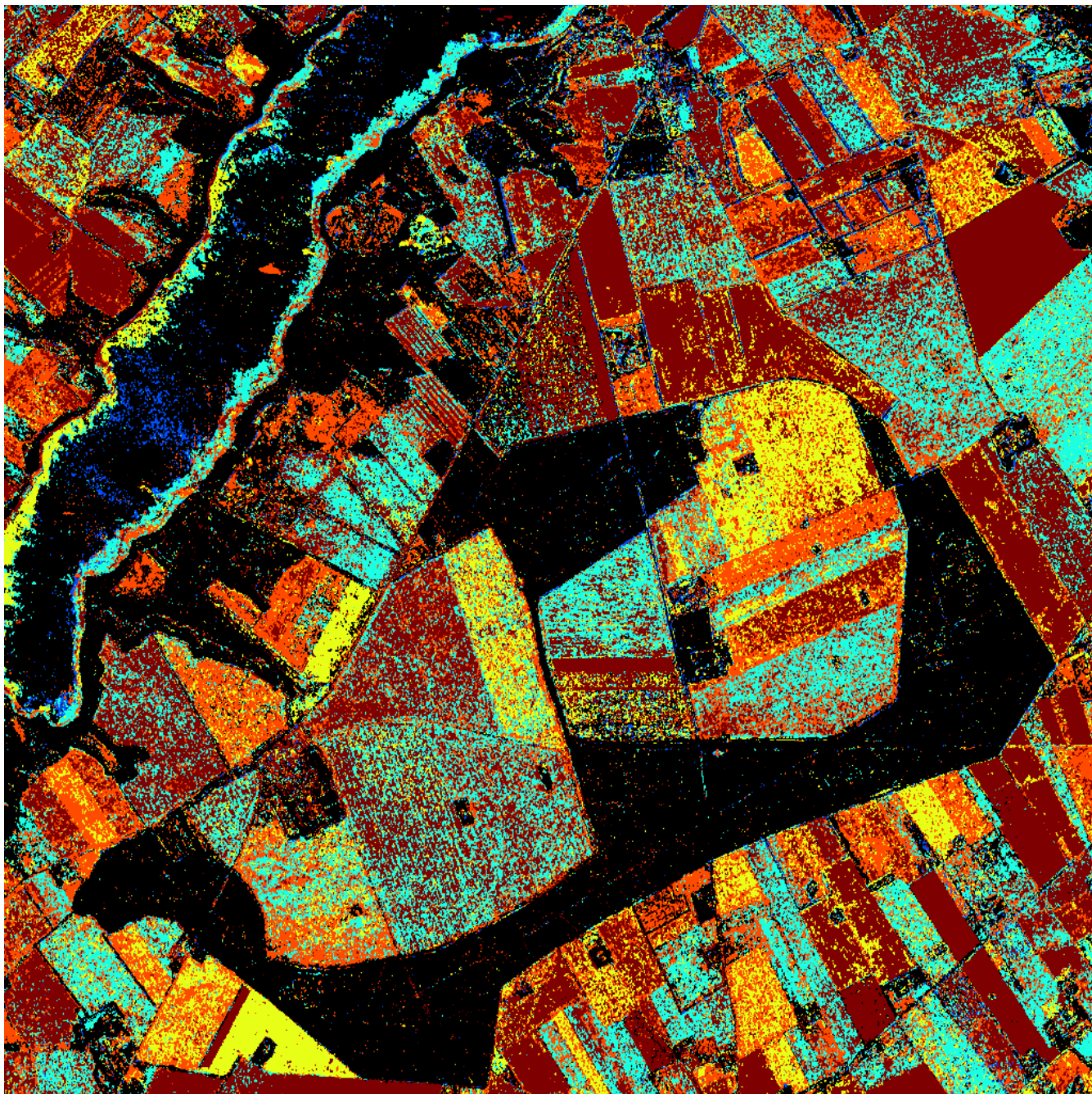
Figure 2: Shows when the last /most recently detected change occurred, zero (black) means no change over the time span, one means first change occurred between t_1 and t_2, etc. Change probability significance level (for full polarization data) is 99.99%.
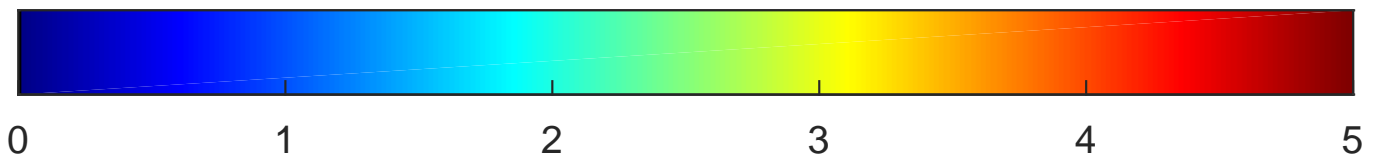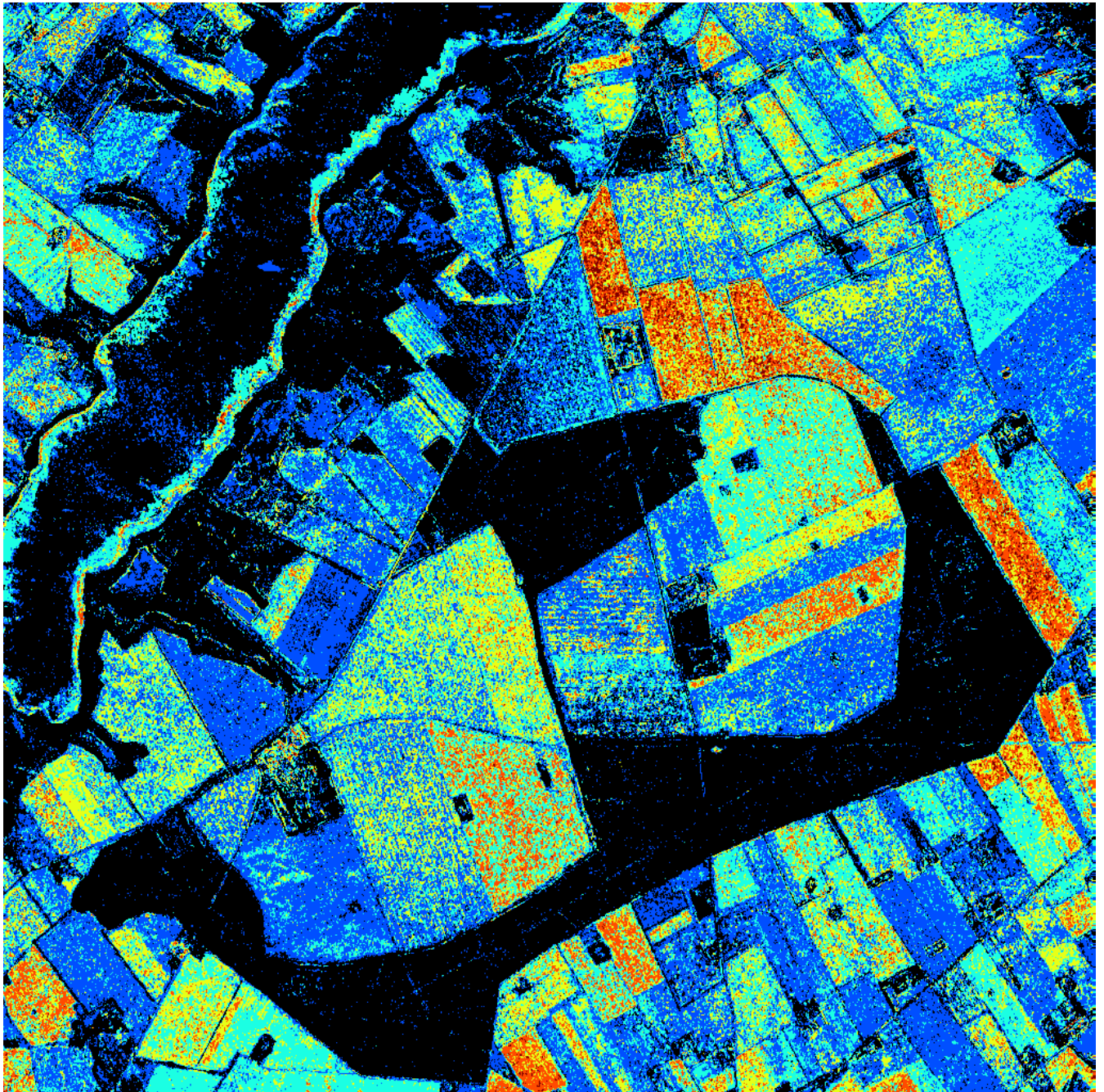
Figure 3: Shows the number of changes/change frequency, again zero (black) means no change. Change probability significance level (for full polarization data) is 99.99%.
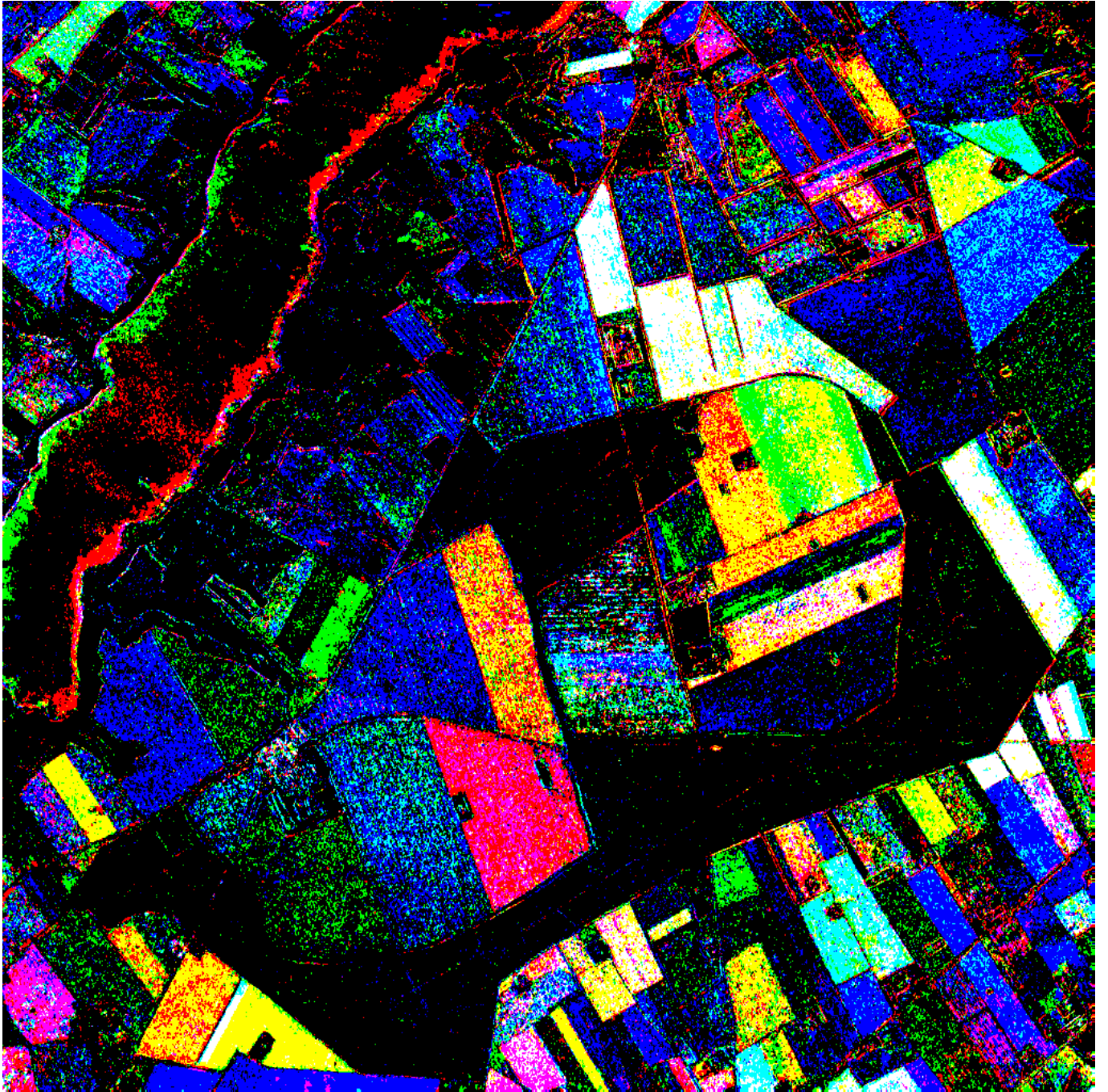
Figure 4: Shows changes from t_1 to t_2 as red, from t_3 to t_4 as green, from t_5 to t_6 as blue (black means no change in the time intervals depicted). Change probability significance level (for full polarization data) is 99.99%.
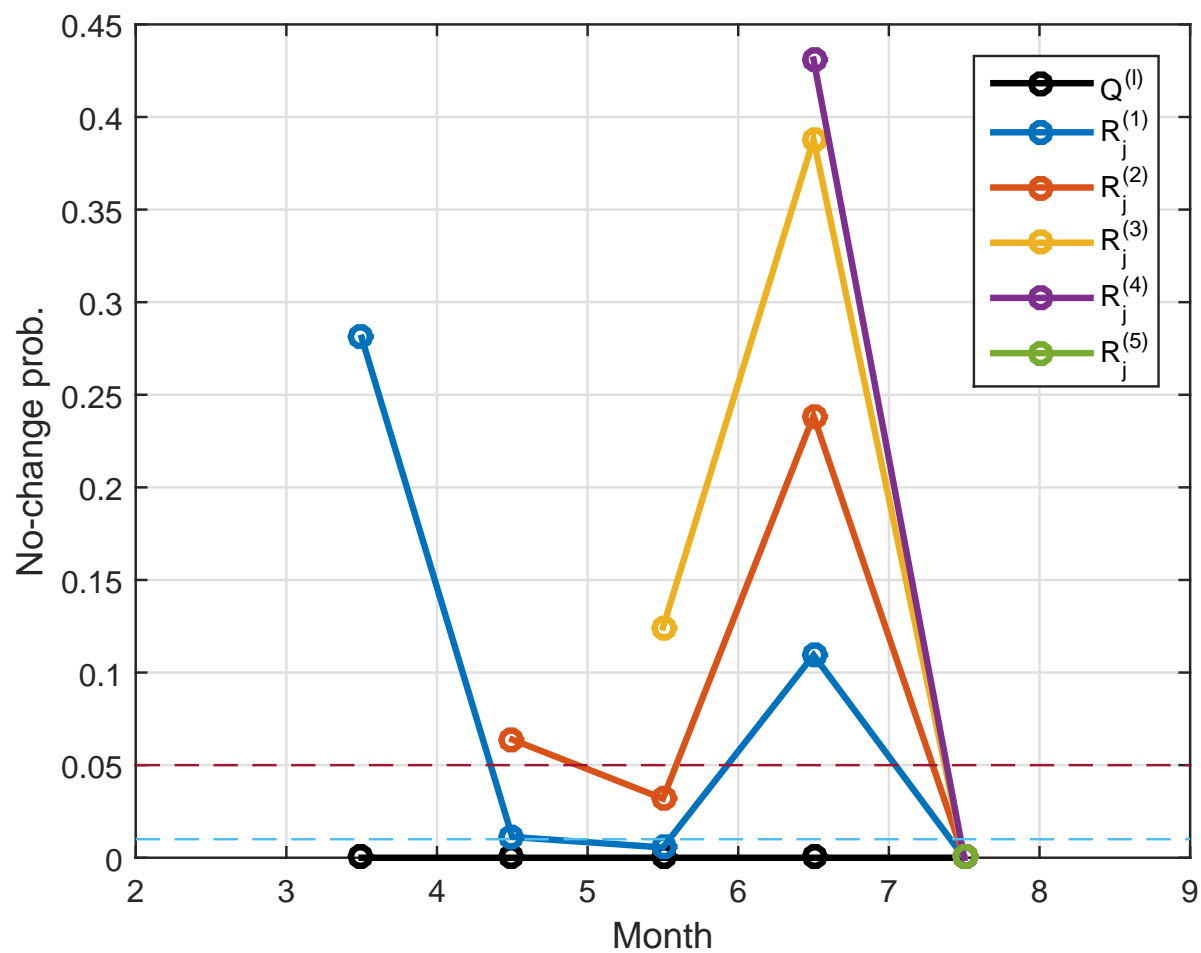
Figure 5: For a grass field this figure shows average omnibus test based no-change probabilities tabulated in Table 2.
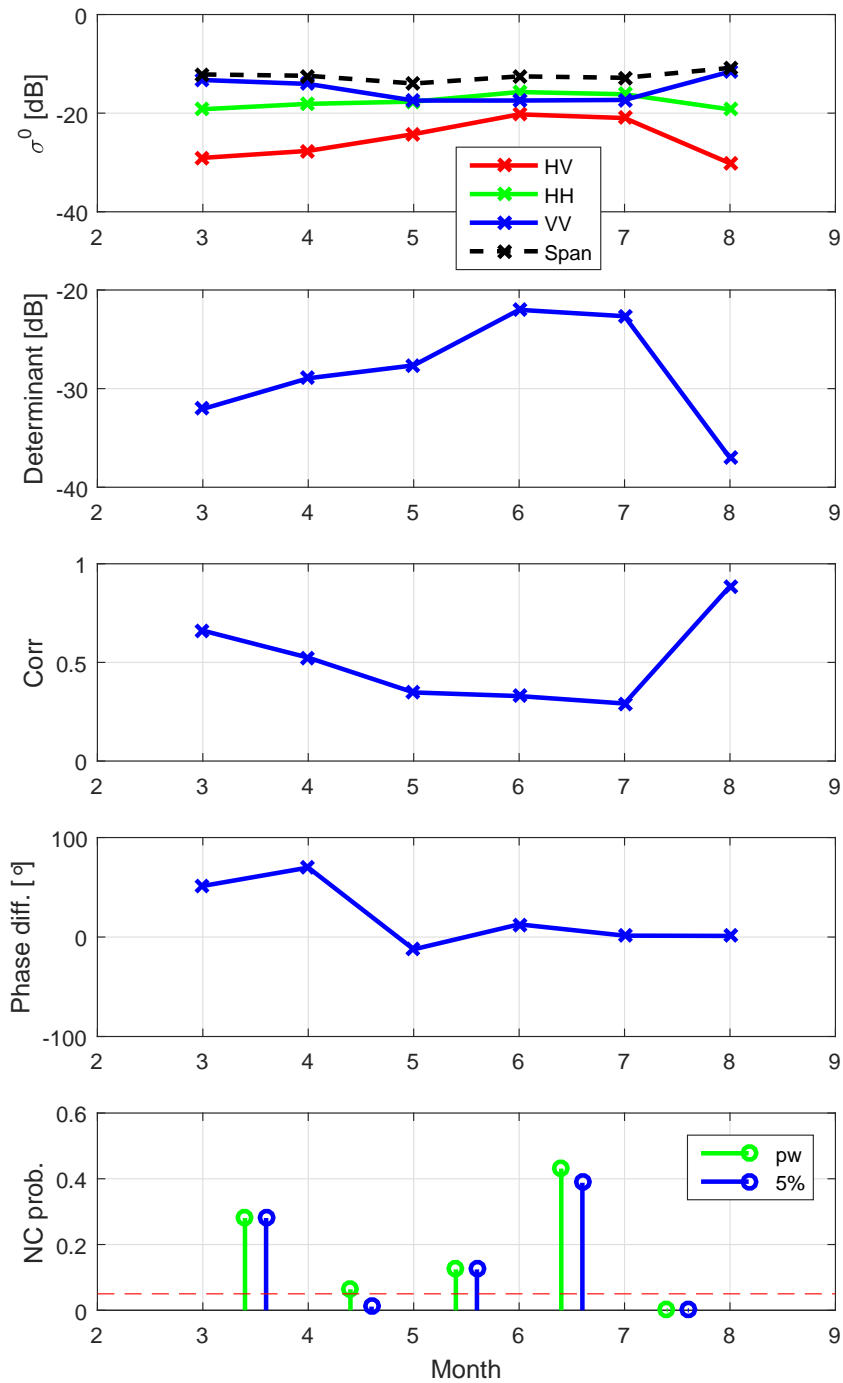
Figure 6: For a grass field this figure shows average (first plot) backscatter coefficients and span, (second plot) determinant of the covariance matrix multiplied by the equivalent number of looks, (third plot) magnitude of the correlation between HH and VV, (fourth plot) phase difference between HH and VV, and (fifth plot) pairwise (green stems) and omnibus test based no-change probabilities (at a 5% significance level, blue stems).
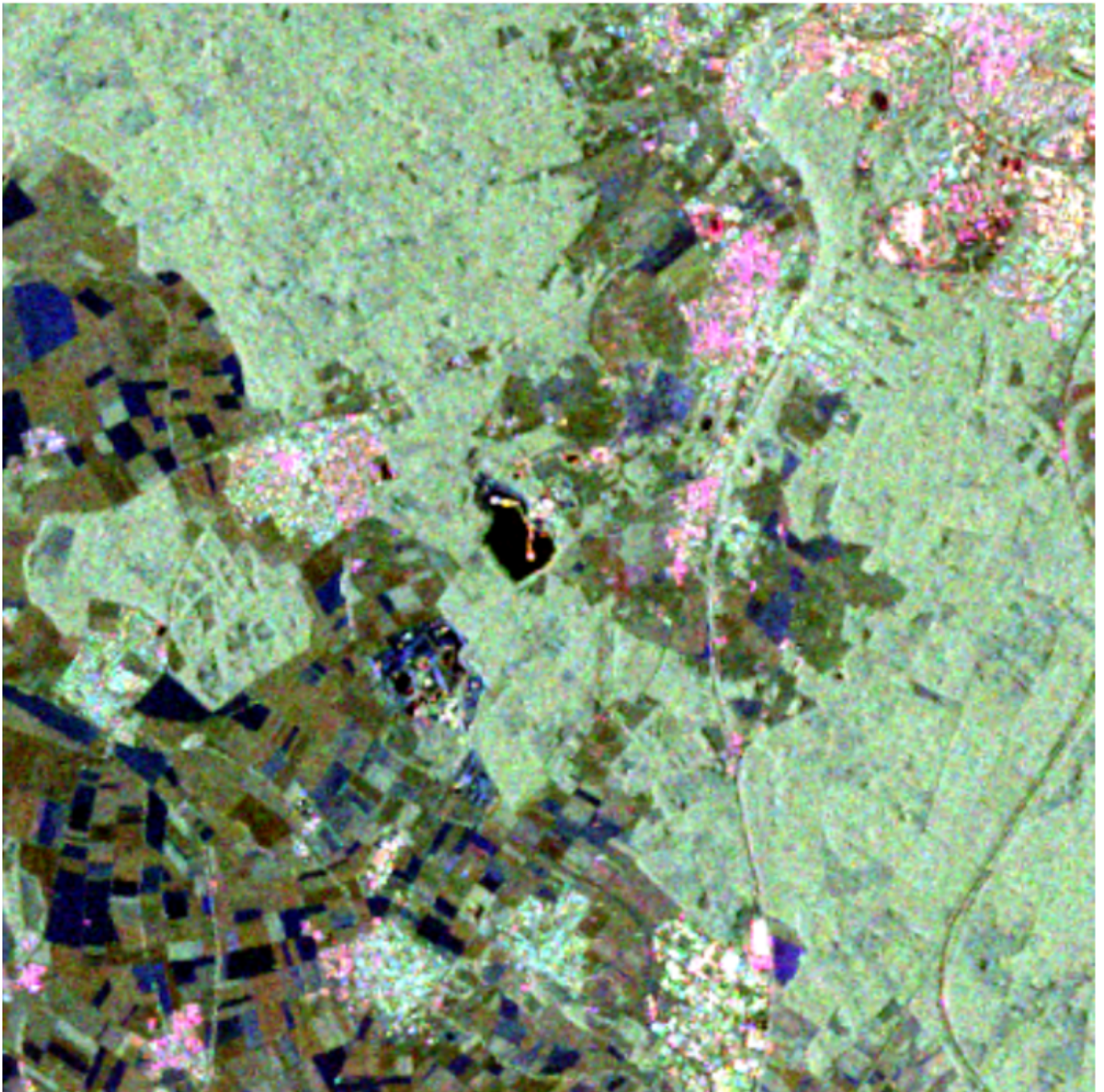
Figure 7: RGB color composite of a quad polarimetric RADARSAT-2 image acquired over an area southwest of Bonn, Germany on May 25, 2009, in the Pauli representation (R = $\langle|S_{hh} - S_{vv}|^2\rangle$ indicating double bounce, G = $\langle|S_{hv}|^2\rangle$ indicating volume scattering, and B = $\langle|S_{hh} + S_{vv}|^2\rangle$ indicating surface scattering or single bounce). RADARSAT-2 Data and Products ©MacDonald, Dettwiler and Associates Ltd. (2009-2010) - All Rights Reserved. RADARSAT is an official trademark of the Canadian Space Agency.
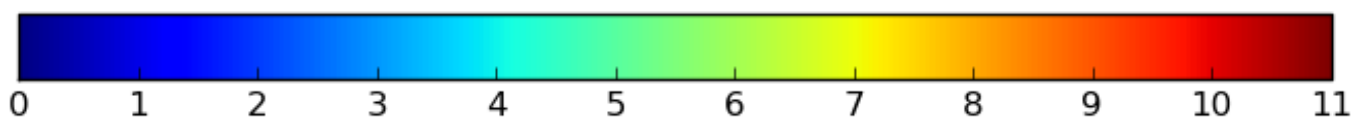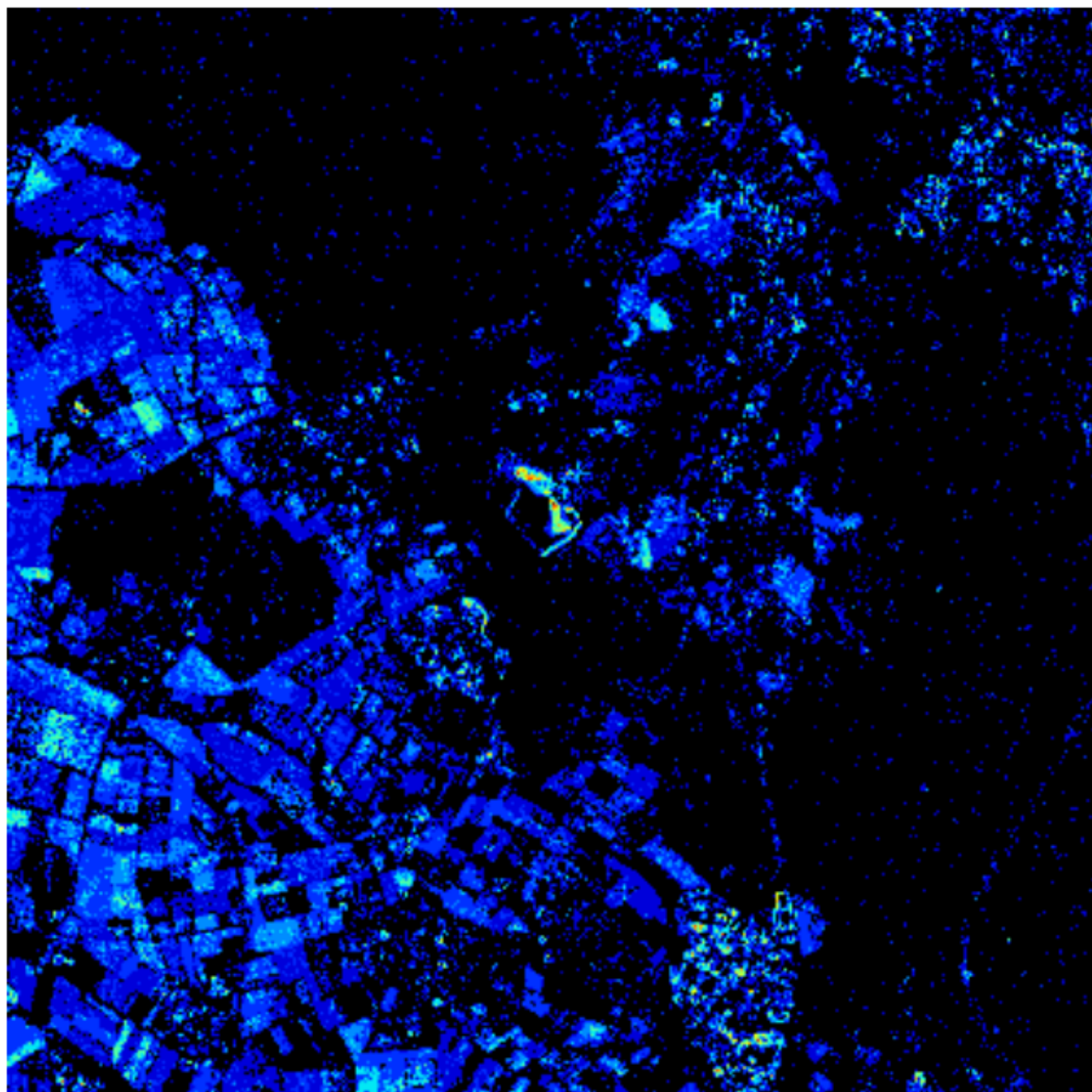
Figure 8: Change frequency map for a series of 12 RADARSAT-2 images acquired between May 25, 2009 and October 11, 2010 (same spatial subset as Figure 7). Change probability significance level is 99.99%. RADARSAT-2 Data and Products ©MacDonald, Dettwiler and Associates Ltd. (2009-2010) - All Rights Reserved. RADARSAT is an official trademark of the Canadian Space Agency.
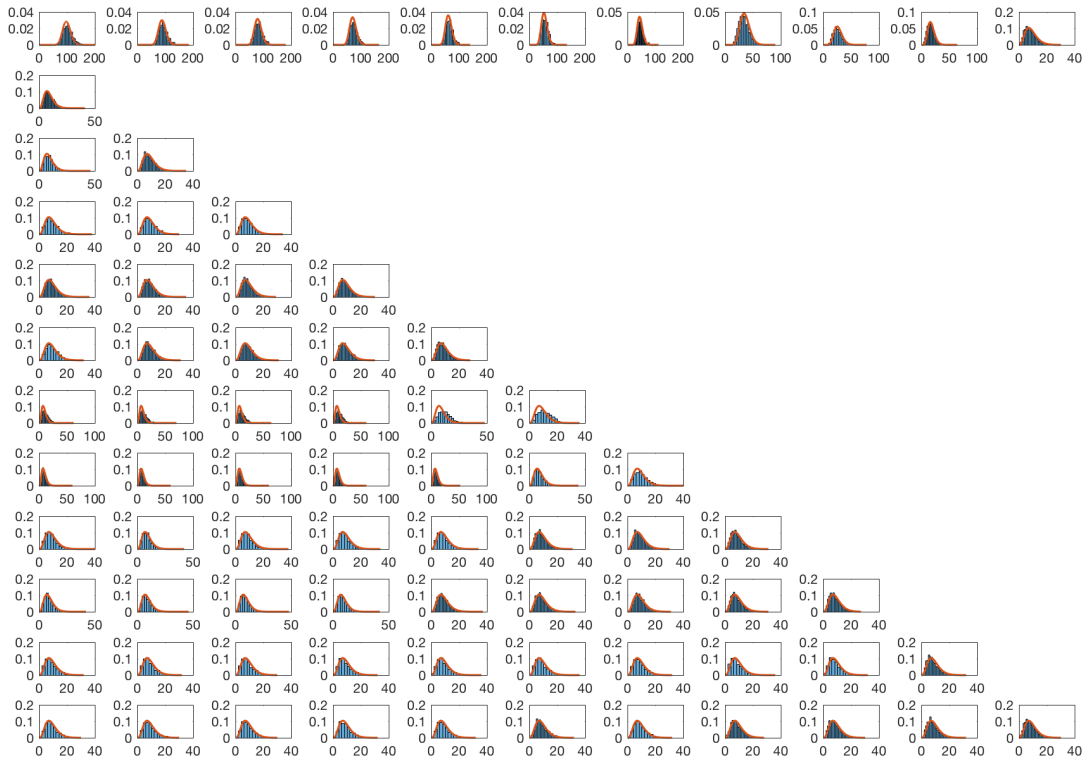
Figure 9: Histograms for an analysis of omnibus change for the RADARSAT-2 data along with the theoretical distributions for a no-change wooded area. For the $-2\rho \ln Q$ (top row plots) the distributions are weighted sums of two χ^2 distributions, see Conradsen et al. (2016). The numbers of degrees of freedom are 99 and 103, 90 and 94, ..., 9 and 13, respectively. For all the $-2\rho_j \ln R_j$ (the remaining rows) the distributions are again weighted sums of two χ^2 distributions, the numbers of degrees of freedom are 9 and 13. Judged visually this illustrates a satisfactory fit between sample histograms and theoretical distributions for the test statistics in a no-change region.